Journal of Hazardous Materials 192 (2011) 1597–1608

Contents lists available at ScienceDirect

Journal of Hazardous Materials

journal homepage: www.elsevier.com/locate/jhazmat

# Remotion of the antibiotic tetracycline by titania and titania–silica composed materials

Maximiliano Brigante*, Pablo C. Schulz

*INQUISUR, Departamento de Química, Universidad Nacional del Sur, Av. Alem 1253, (8000) Bahía Blanca, Argentina*

ARTICLE INFO

*Article history:*
Received 30 April 2011
Accepted 28 June 2011
Available online 2 July 2011

*Keywords:*
Tetracycline
Mesoporous materials
Adsorption
Electrostatic interactions
H-bonding
Photodegradation kinetics

ABSTRACT

Removal of the antibiotic tetracycline (TC) by $TiO_2$ and the mesoporous binary system $TiO_2$–$SiO_2$ have been studied in batch experiments by performing adsorption isotherms/kinetics and photodegradation kinetics under different conditions of pH, supporting electrolyte concentration, temperature, adsorbent amount, and $TiO_2$-loading. On the one hand, the adsorption of TC on the studied materials is strongly dependent on pH, increasing as pH decreases. The adsorption mechanism, controlled by diffusion processes, is strongly related to electrostatic attractions and H-bond formations mainly between amide, carbonylic and phenolic groups of the antibiotic and the functional groups of $TiO_2$. The adsorption capacity at constant pH increases in the order $TiO_2$ < $TiO_2$–$SiO_2$ mainly due to the highly surface area that the silica offers and to the homogenously dispersion of the $TiO_2$ nanocrystallites. On the other hand, the photodegradation rate is affected by the presence of the studied materials at several pH, although its photocatalytic activities are more important at pH 7 or lower. The photodegradation mechanisms seem to be related to the formation of $OH^{\bullet}$ radicals which are responsible for the decomposition of TC. The composed titania–silica materials might act not only as an excellent adsorbent but also act as an alternative photocatalyst for pollution control.

© 2011 Elsevier B.V. All rights reserved.

## 1. Introduction

Pharmaceutical antibiotics are used extensively worldwide in human therapy and the farming industry. In the United States alone, the annual antibiotic production was estimated to be 227 million kilograms in 2000 [1]. The antibiotics administered are often poorly metabolized and absorbed by humans and animals and, therefore, tend to enter the aquatic environment [2–4]. Exposure to residues of antibiotics and their transformed products might cause a variety of adverse effects, including acute and chronic toxicity and microorganisms antibiotic resistance [5,6]. However, the removal of antibiotics by conventional water treatment technologies is incomplete [7,8]. Hence, there is an increasing demand for developing more effective treatment technologies to remove pharmaceutical antibiotics from water.

Removal of antibiotics and other anthropogenic compounds by adsorption is considered the major cause of pollutant deactivation and it is important from the point of view of both inhibiting their toxic properties and restricting their transport into water systems. A widely variety of solids such as clays, metal oxides and activated carbon have been used for those purposes. Some of them are good adsorbents in certain experimental conditions but have little or no capacity to adsorb in natural conditions [9], which facilitates the antibiotic leaching into groundwaters. On the contrary, other solids have high affinity for contaminants, protecting them in the adsorbed state from the attack of microorganisms and preventing its degradation [10]. Due to its strong adsorption affinity and relatively low cost, activated carbon has been commonly used as an effective adsorbent for many antibiotics. However, this material has several disadvantages such as (a) inactive towards hydrophilic and/or electrical-charged molecules, (b) predominantly consists of micropores (<2 nm in size) with irregular-shape, closed pore structures, where the adsorption of bulky organic chemicals might be greatly impeded by the size exclusion effect, (c) the working capacity decreases in the presence of natural organic matter, and (d) its regeneration is questionable [11,12]. Other of the widely used materials is titanium dioxide or titania ($TiO_2$) due to its high photocatalytic activity, low cost, nontoxicity and high stability in aqueous solution [13]. Neverthless, $TiO_2$ powders have disadvantages such as low surface area (Degussa P25 = 35–45 $m^2\,g^{-1}$, anatase = <10 $m^2\,g^{-1}$); a large band gap (3.20 eV for anatase) and therefore only a small UV fraction of solar light, about 2–3%, can be used; and the separation and recovery of $TiO_2$ powders from wastewater are difficult [14,15]. For these reasons, researchers have focused their attention on the synthesis of new materials for pollutant remotion, mainly on solids with high surface area, pore size and catalytic activity.

* Corresponding author. Tel.: +54 291 4595101x3523.
*E-mail address:* brigante@uns.edu.ar (M. Brigante).

0304-3894/$ – see front matter © 2011 Elsevier B.V. All rights reserved.
doi:10.1016/j.jhazmat.2011.06.082

The adsorptive and photocatalytic properties of $TiO_2$ can be improved by the incorporation of the titania on/into nonreactive, photoinert support materials. In this aspect, mesoporous silica can act as support due to its high surface area (>200 $m^2\,g^{-1}$), ordered frameworks, narrow pore size distribution (2–>10 nm, higher than zeolites), and high thermal stability [16–18]. In fact, it has been reported that the $TiO_2$ supported on these materials significantly enhances its catalytic activity towards different dyes in comparison to the pure oxide [19]. Similar results were reported by Sharma et al. [20,21] on the degradation of three herbicides on $TiO_2$/porous silica nanoparticles systems. Another procedure that have been used to increase the activity of commercial $TiO_2$ is the synthesis of mesoporous titania. The first materials were obtained in 1995 [22]. However, the synthesis of mesoporous $TiO_2$ is more complicated than the case of silica, due to a rapid hydrolysis and condensation of the metal, resulting in poorly structured and non-porous materials [23].

The aim of this article is divided in two parts. First, to present a study of the adsorption (kinetics and equilibrium experiments) of tetracycline on $TiO_2$ and mesoporous $TiO_2$–$SiO_2$ composed materials. The second part involves the study of the photodegradation kinetics of tetracycline in presence and absence of the studied materials under a UV lamp. The data obtained at a variety of pH, temperatures, ionic strengths, adsorbent amount, and $TiO_2$-loading are used to gain insights into the mechanisms that govern the adsorption and photodegradation and into the factors that promote or prevent both processes. Tetracycline (TC) is an antibiotic that exhibit broad-spectrum antimicrobial activities against a variety of disease producing bacteria. The maximum permissible concentration of TC in aqueous solutions for industrial and pharmacy wastewaters is very low (1 $\mu g\,L^{-1}$) although concentrations of 0.52 $\mu g\,L^{-1}$ in influents and 0.17 $\mu g\,L^{-1}$ in effluents have been reported [24,25]. It bears different charges on different sites depending on solution pH as shown in Fig. 1. At pH below 3.3, the dimethylammonium group is protonated, resulting in a cationic form of +00. Between pH 3.3 and 7.7, it exists as a zwitterion, +−0 (which predominates and reaches a maximum concentration at pH 5.0), due to the loss of proton from the phenolic diketone moiety. When pH is above 7.7, it is present as a monovalent anion, +−−, or a divalent anion, 0−−, due to the loss of protons from the tricarbonyl system and phenolic diketone moiety [26,27]. Its $pK_{a1}$, $pK_{a2}$, $pK_{a3}$ values in aqueous solutions are 3.3, 7.7, 9.7, respectively.

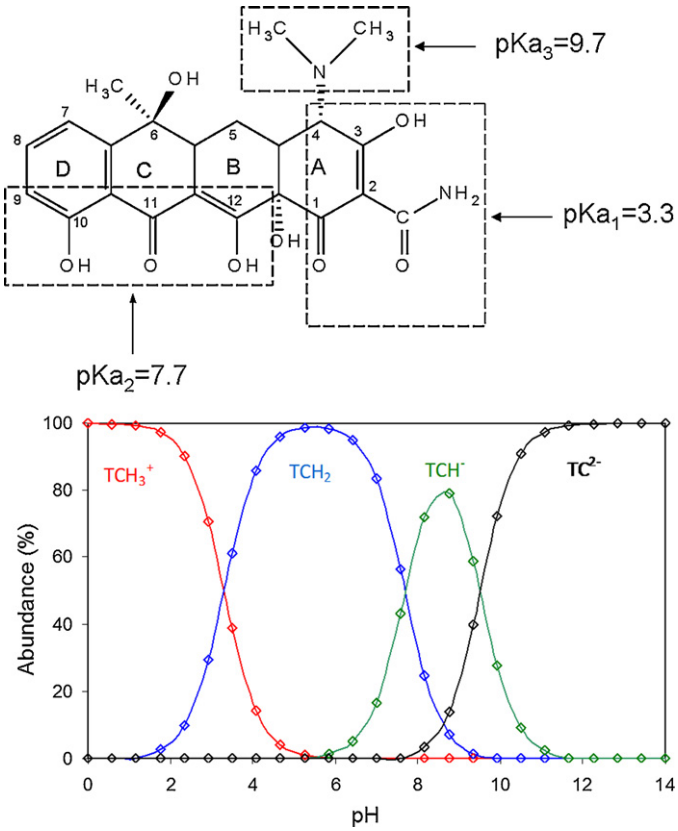


**Fig. 1.** Molecular structure of TC and its speciation under different pH values in aqueous solution.

## 2. Materials and methods

### 2.1. Chemicals

Sodium dioctyl sulfosuccinate (Aerosol OT, AOT) 99%, tetraethyl orthosilicate (TEOS, 99%), hexadecyl (=cetyl) trimethylammonium bromide (CTAB), and commercial $TiO_2$ (anatase 99%) were obtained from Aldrich. $TiCl_4$ (99%, $\delta = 1.722\,g\,cm^{-3}$) and n-hexane were purchased from Carlo Erba. NaOH, sodium acetate, acetic acid, sodium carbonate, sodium hydrogen carbonate, disodium phosphate anhydrous, and monosodium phosphate anhydrous were obtained from Anedra. All chemicals were of analytical grade and used as received. Tetracycline hydrochloride was obtained from PARAFARM, and its purity (99%) was confirmed by XRD and FT-IR spectroscopy. Doubly distilled water was used for the preparation of solutions for experiments.

### 2.2. $SiO_2$–$TiO_2$ materials. Synthesis and general characterization

Synthesis of $TiO_2$, $SiO_2$, and composed $TiO_2$–$SiO_2$ materials were carried out using a procedure similar to that described by Messina et al. [28]. The $TiO_2$ content on the silica support was 9, 28 and 51 wt%, which was confirmed by XRD and SEM-EDX (see below).

The synthesized materials were characterized by the techniques usually employed in porous materials, such as scanning and transmission electron microscopy, X-ray diffraction (XRD), FT-IR and the $N_2$-BET method for surface area, pore volume and pore diameter determination. Scanning electron microscopy (SEM) was performed using a LEO 40-XVP microscope equipped with a secondary electrons detector and an X-ray microanalysis system (EDAX DX-4). The samples were prepared on graphite stubs and coated with a ca. 300 Å gold layer in a PELCO 91000 sputter coater. Transmission electron microscopy (TEM) was performed using a JEOL 100 CX II transmission electron microscope, operated at 100 kV with magnification from 50000× to 200000×. Observations were made in a bright field. Powdered samples were placed on cooper supports of 2000 mesh. XRD patterns were collected via a Philips PW 1710 diffractometer with Cu Kα radiation (λ = 1.5406 Å) and graphite monochromator operated at 45 kV, 30 mA and 25 °C. The $N_2$ adsorption isotherms at 77.6 K were measured with a Micrometrics Model Accelerated Surface Area and Porosimetry System (ASAP) 2020 instrument. Each sample was degassed at 373 K for 720 min at a pressure of $10^{-4}$ Pa. FT-IR experiments were recorded in a Nicolet FT-IR Nexus 470 Spectrophotometer. To avoid co-adsorbed water the samples were dried under vacuum until constant weight was achieved and diluted with KBr powder before the FT-IR spectra were recorded.

### 2.3. Adsorption experiments

Adsorption experiments (in darkness to avoid photodegradation) were obtained with a batch equilibration procedure using 15 mL polypropylene centrifuge tubes covered with polypropylene caps immersed in a thermostatic shaker bath. Before starting

an experiment, a stock TC solution ($5 \times 10^{-4}$ M) were prepared by adding the corresponding solid to pH buffer solutions. The pHs used in these studies were 4.4, 7.0, and 9.5 by using 0.1 M acetate/acetic acid, $HPO_4^{-2}/H_2PO_4^{-1}$, and $CO_3^{-2}/HCO_3^{-1}$ buffer solutions, respectively. 50 mg of mesoporous material (except when the effect of adsorbent amount were evaluated) were introduced into the tubes and mixed with varying quantities of TC and KCl (used as supporting electrolyte) solutions. The range of initial TC concentration was 5–400 μM, and the final volume was 8 mL. The stirring speed was kept constant at 90 rpm. At different reaction times, the particles were separated from the supernatant by centrifugation at 4000 rpm during 2 min and the supernatant was immediately analysed to quantify the concentration of adsorbed TC. After the quantification (see below), that took around 30 s, the supernatant was reintroduced into the tube. This procedure (separation, quantification of TC and reintroduction of the supernatant into the reaction tube) was repeated during several hours in order to achieve complete adsorption of the antibiotic or to gather enough data points. The last data point obtained of these experiments was assumed as equilibrium concentration of TC in the supernatant. Adsorbed TC was calculated from the difference between the initial TC concentration and the concentration of the antibiotic that remained in the supernatant solution. In most experiments no supporting electrolyte was used and the working temperature was 25 °C (except when effects of ionic strength and temperature were investigated).

Quantification of TC was performed by UV–vis spectroscopy at 358 nm for pH 4.4 and 7, and at 377 nm for pH 9.5. This is due to the shifting of the maximum absorption band of TC towards higher wavelength as pH increases. Quantification of dissolved HA was performed by UV–vis spectroscopy, using an Agilent 8453 UV–vis diode array spectrophotometer equipped with a Hellma 1 cm quartz cell. The supernatant of the withdrawn aliquot was placed into the cell and the spectrum was recorded in the 200–900 nm wavelength range. Calibration curves at the working pH were also constructed with several TC solutions having concentration that ranged between $5 \times 10^{-6}$ and $1 \times 10^{-3}$ M. Very good linearity was found in all cases.

The adsorption isotherms were fitted using the Langmuir and Freundlich equations, which were commonly used in the adsorption of antibiotics on several adsorbent systems [8,29]. The linear forms of these equations are displayed as equations (1) Langmuir and (2) Freundlich:

$$\frac{1}{TC_{ads}} = \frac{1}{q_{mon} K_L TC_{eq}} + \frac{1}{q_{mon}}, \quad (1)$$

$$\ln TC_{ads} = \ln K_F + \frac{1}{n} \ln TC_{eq}, \quad (2)$$

where $TC_{ads}$ is the adsorbed amount of TC (μmol g$^{-1}$); $TC_{eq}$ is the equilibrium concentration of TC in the supernatant (μM); $q_{mon}$ is the maximum amount of antibiotic adsorbed (μmol g$^{-1}$) corresponding to complete coverage on the surface; $K_L$ and $K_F$ are the Langmuir and Freundlich constants (μM$^{-1}$), respectively; and $1/n$ is the adsorption intensity. From the linearized form of Eqs. (1) and (2), $q_{mon}$, $K_L$, $K_F$, $1/n$, and the correlation coefficient, $r^2$, can be calculated.

The adsorption kinetics is traditionally described following the expressions originally given by Lagergren, which are special cases for the general Langmuir rate equation [30]. Simple kinetic analyses of adsorption are the pseudo-first and the pseudo-second order equations in their integrated form:

$$\ln(q_e - q_t) = \ln q_{eq} - k_{1,s} t, \quad (3)$$

$$\frac{t}{q_t} = \frac{1}{k_{2,s} q_e^2} + \frac{1}{q_e} t. \quad (4)$$

where $k_{1,s}$ is the pseudo-first-order constant (min$^{-1}$), $k_{2,s}$ and is the pseudo-second-order rate constant (g μmol$^{-1}$ min$^{-1}$); and $q_e$ and $q_t$ (μmol g$^{-1}$) denote the amount of antibiotic adsorbed at equilibrium and at the reaction time $t$, respectively. The fitting validity of these models is traditionally checked by the linear plots of $\ln(q_e - q_t)$ versus $t$ and $t/q_t$ versus $t$, respectively. The slope and intercept of the obtained straight line provide the respective kinetic constant and the $q_e$ parameters.

Despite the Lagergren kinetic equations have been used for a great deal of adsorption kinetic works, this model cannot give interaction mechanisms, so another model to test antibiotic adsorption on the studied materials was also used. A pore diffusion model, described by Eq. (5), was used here and in most solid/solution interaction studies [31]:

$$\ln q_t = k_{diff} t^{-1/2} + I, \quad (5)$$

where $k_{diff}$ is the pore diffusion rate constant (μmol g$^{-1}$ min$^{-1/2}$) and $I$ is the intercept (μmol g$^{-1}$). If the adsorption mechanism follows the pore diffusion processes a plot of $\ln q_t$ versus $t^{-1/2}$ should be a straight line with a slope $k_{diff}$ and intercept $I$.

### 2.4. Photodegradation kinetics

To study the effect of the photodegradation, the same experiments were carried out in presence of UV light at 25 °C. A DESAGA UV 131000 lamp (λ = 366 nm) was used as an irradiation source for the photodegradation of TC. Light intensity was estimated as $I_a = 2.7 \times 10^{-6}$ molphotons$^{-1}$ [32]. To discriminate between both effects (adsorption and photodegradation) the results of the experiments without light were subtracted from those carried out under irradiation. Two kinetic models, i.e. the first-order equation and the second-order equation were considered for interpreting the experimental data:

$$\ln \frac{TC_0}{TC_t} = -k_1 t, \quad (6)$$

$$\frac{1}{TC_t} - \frac{1}{TC_0} = k_2 t, \quad (7)$$

where $k_1$ is the first-order constant (min$^{-1}$), $k_2$ is the second-order constant (μM$^{-1}$ min$^{-1}$); and $TC_0$ and $TC_t$ indicate the concentration of TC supernatant (μM) at $t = 0$ and $t = t$, respectively.

## 3. Results and discussions

### 3.1. Characterization of synthesized materials

Characterization of the obtained materials by the techniques mentioned above was showed in Supplementary Material, SM. SM Fig. S1 shows the X-ray diffractogram of $SiO_2$, $TiO_2$ and 28 wt% $TiO_2$–$SiO_2$ materials. $SiO_2$ shows a typical amorphous XRD patterns which are characteristic of mesoporous silicas [21]. This means that the mesoporous structure of $SiO_2$ is stable under our synthesis conditions and it does not collapse during calcination at 540 °C resulting in transformation to the cristobalite phase [33]. Titania shows several diffraction peaks, relating to the formation of a mixed phase composed by anatase and rutile [19] in a 5:1 molar ratio. However, the rutile diffraction peaks disappear in the XRD patterns of 28 wt% $TiO_2$–$SiO_2$ (as well as in 9 and 51 wt%, data not shown) evidencing that anatase is the only titania crystalline phase. The rutile phase is essentially formed at higher calcination temperatures (>450 °C) [34]. However, the non-appearance of rutile diffraction peaks in $TiO_2$–$SiO_2$ materials are in agreement with Yang et al. [35], who reported that silica plays a key role in the inhibition of the formation of rutile phase. It is also interesting to note that supported $TiO_2$ shows broad diffraction peaks in comparison to bare titania,

suggesting the formation of dispersed $TiO_2$ nanocrystallites [36]. In fact, the grain sizes of free and supported $TiO_2$, determined from the width at half maximum of the anatase (1 0 1) peak according to the Scherrer formula [37], are 13 and 4 nm, respectively. These values of grain size are consistent with the TEM studies.

The morphology of the studied samples was also investigated by SEM and TEM techniques and the respective micrographs are presented in SM Fig. S2. $SiO_2$ (SM Fig. S2a) shows randomly shaped aggregates of variable size and these do not provide a clear morphology. TEM image (SM Fig. S2b) seems to show a typical hexagonal arrangement of mesopores whose dimensions may be engineered in the range of ~18 nm. $TiO_2$ particles also show randomly shaped aggregates probably due to a faster condensation of titania (SM Fig. S2c). The aggregates are formed by nanoparticles whose average diameter was 15 nm. The structure of the particles seems to be tetrahedrical instead of rhombic (SM Fig. S2d). This means that the structure of particles is that of rutile or anatase, not that of brookite [28]. The morphology of 28 wt% $TiO_2$–$SiO_2$ (SM Fig. S2e) is similar to that of the bare silica and it does not show clearly titania crystallites. This may indicate the formation of fine particles and dispersion of $TiO_2$ over the support or into the mesopores [21]. From the TEM images it appears that $TiO_2$ nanoparticles (black spot) are distributed in both the pores and on the pore walls (SM Fig. S2f). The diameter of titania nanoparticles on the mesopores structure is at around 5–7 nm, which is smaller than titania particles obtained by calcination. This may mean that calcination produces synterization of the particles, whilst the presence of the silica structures produces separation of the original particles and avoids the synterization [28].

The nitrogen adsorption–desorption isotherms of the studied materials are shown in SM Fig. S3. Briefly, it shows that $SiO_2$ (ii) and 28 wt% $TiO_2$–$SiO_2$ (iii) represent typical type IV isotherms with a H2 hysteresis loop that is characteristic of mesopores [28]. Similar results were obtained for 9 and 51 wt% $TiO_2$–$SiO_2$. However, the adsorption/desorption isotherms on $TiO_2$ (i), and anatase (data not shown) are type II [38]. It represents unrestricted monolayer–multilayer adsorption. There is a hysteresis of type H4, which is associated with narrow slit-like pores. Similar results were reported by Zubieta et al. in porous $TiO_2$ and $TiO_2$–chitosan materials [31]. In the case of slit-like pores, the determined diameter is the pore width. Specific surface area, pore diameter, and pore volume of the solids are summarized in Table 1. The average pore diameter of $SiO_2$ was at around of 18 nm, which is in agreement to those reported in TEM microscopy. Table 1 also shows that change in $TiO_2$ content in the silica structure results in important changes in the surface area and pore diameter. On the one hand, the surface slightly decreases in 9 wt% $TiO_2$–$SiO_2$ in comparison to bare silica and then it increases as $TiO_2$-loading increases. These changes seem to be attributed to the incorporation of titania particles into the mesopore structure (decrease in $A_{BET}$) followed to the start growing of the $TiO_2$ crystallites on the outer surface of $SiO_2$ at higher titania-loading (increase in $A_{BET}$) [39]. On the other hand, the pore size in $TiO_2$–$SiO_2$ increases in the order 9 wt% < 28 wt% < 51 wt% which may be probably attributed to an increased contribution of the naked titania character in the samples with the increasing of $TiO_2$-loading [35].

FT-IR spectra of $SiO_2$, $TiO_2$ and 28 wt% $TiO_2$–$SiO_2$ are shown in SM Fig. S4. The most important features of $SiO_2$ are a broad band centered at 3625 $cm^{-1}$ associated to OH stretch from surface hydroxyls bound to silica (Si–OH), a broad peak located at 1091 $cm^{-1}$ which is attributed to asymmetric Si–O–Si vibrations, two peaks centered at 797 and 622 $cm^{-1}$ due to symmetric Si–O–Si vibrations, and a peak centered at 478 $cm^{-1}$ assigned for Si–O–Si bending modes [40]. $TiO_2$ shows characteristic absorption bands at around 3478, 1633 (shoulder), 1123, and 486 $cm^{-1}$ which are attributed to O–H stretching vibration of the adsorbed water and hydroxyl groups on the surface, O–H bending, Ti–O stretching and Ti–O–Ti vibrations, respectively [19]. Some differences can be observed in the FT-IR spectrum of $TiO_2$–$SiO_2$. One such difference is the decrease in the intensity of the 797 and 622 $cm^{-1}$ peaks (the last peak decreases up to disappear), corresponding to the symmetric Si–O–Si vibrations. In addition, the band situated at 1091 $cm^{-1}$ corresponding to asymmetric Si–O–Si vibrations is shifted towards lower wavenumbers with decrease in broadness. Several works have described a new peak located at 960 $cm^{-1}$ which is attributed to Ti–O–Si vibrations [40,41]. This peak appears in our spectra as a shoulder in the broad peak located at around 1110 $cm^{-1}$ in all studied titania–silica materials. These changes in the FT-IR spectra are significant evidences that $TiO_2$ interacts with the silica support through chemical bonding, similar as those reported in several reviews [42,43].

### 3.2. Adsorption studies

Fig. 2 shows the effects of pH on the adsorption kinetics of TC on 28 wt% $TiO_2$–$SiO_2$ and $TiO_2$ at 25 °C and 0 M ionic strength. All curves have similar characteristics, showing an important and fast adsorption between $t = 0$ and 5 min, and a slower adsorption at longer times. Although adsorption seems to reach completion at around 250 min, some long-term kinetic experiments revealed that adsorption continues after several days, but very slowly. It also shows that the adsorption on both adsorbents is strongly

**Table 1**
Nitrogen adsorption results on the studied solids.

| Sample | $A_{BET}$ ($m^2g^{-1}$) | $D_{aap}$ (nm) | $V_{spat}$ ($cm^3g^{-1}$) |
|---|---|---|---|
| $SiO_2$ | 238.6 | 18.89 | 0.4104 |
| 9%wt $TiO_2$-$SiO_2$ | 234.8 | 5.65 | 0.3544 |
| 28%wt $TiO_2$-$SiO_2$ | 259.2 | 7.77 | 0.4003 |
| 51%wt $TiO_2$-$SiO_2$ | 274.0 | 12.35 | 0.3093 |
| $TiO_2$ | 9.5 | 21.09 | 0.0499 |
| anatase | 9.9 | 10.07 | 0.0250 |

*Note*: $A_{BET}$: BET surface area; $D_{app}$: adsorption average pore diameter by BET (8V/A); $V_{spat}$.: single point adsorption total pore volume of pores.

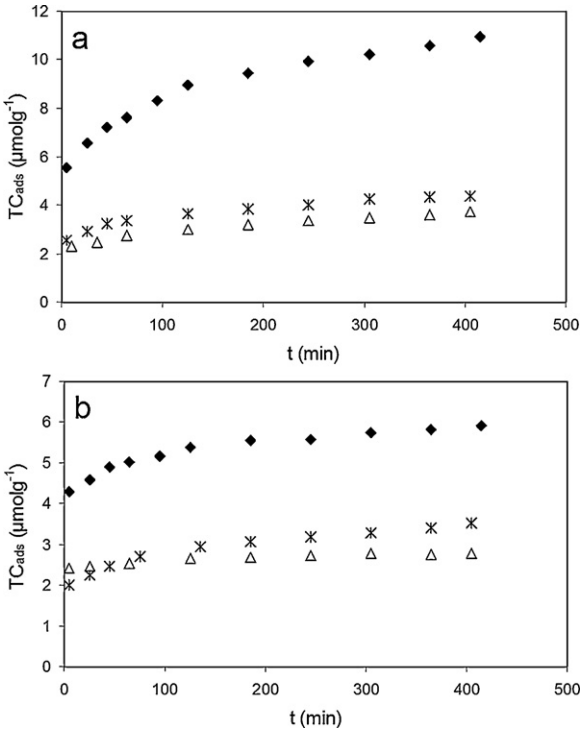


**Fig. 2.** Effect of pH on the adsorption kinetics of TC on (a) 28 wt% $TiO_2$–$SiO_2$, and (b) $TiO_2$ at 25 °C. pH values: solid diamonds, pH 4.4; stars, pH 7.0; open triangles, pH 9.5.

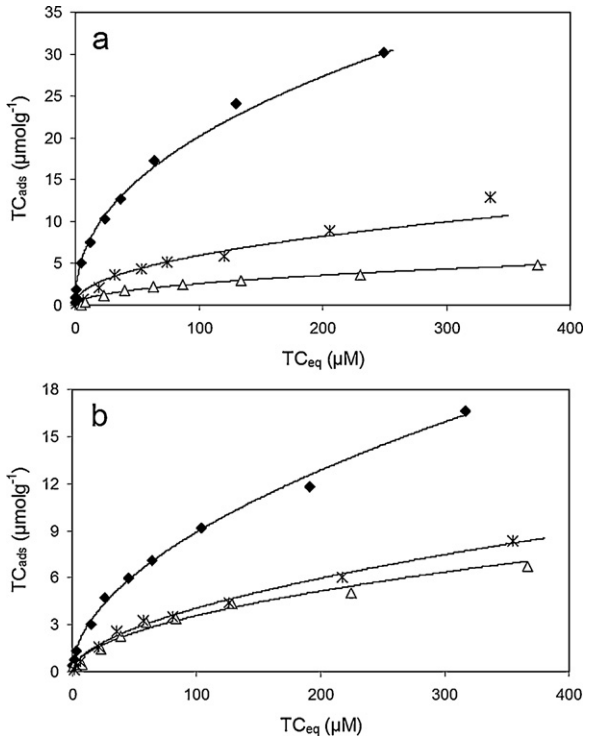


**Fig. 3.** Effect of pH on the adsorption of TC on (a) 28 wt% $TiO_2$–$SiO_2$, and (b) $TiO_2$ at 25 °C. pH values: solid diamonds, pH 4.4; stars, pH 7.0; open triangles, pH 9.5. Lines show predictions of Eq. (2) with parameters from Table 1.

dependent on the pH. It is relatively high at low pH and decreases significantly at higher pH values. The adsorption of TC on $SiO_2$ and anatase (data not shown) is very low and only detectable at pH 4.4. The effect of pH can be better observed in the respective adsorption isotherms shown in Fig. 3. As expected, the adsorption is relatively high at pH 4.4 and decreases significantly at pH 7 and 9.5 indicating that the affinity of TC for both adsorbents surface is higher at low pH.

TC adsorption on $TiO_2$–$SiO_2$ seems to take place either by direct binding to the uncovered $SiO_2$ surface or by direct binding to the supported $TiO_2$. The first case appears to be less important under our experimental conditions since it was reported that attachment to the bare silica surface is very low. The second case seems to be the most probable. The direct binding between TC and $TiO_2$ generates ternary surface species TC–$TiO_2$–$SiO_2$, whose formation is mainly driven by TC–$TiO_2$ interactions. The direct binding between TC and $TiO_2$ can be better visualized comparing the FT-IR spectra of titania and TC adsorbed on $TiO_2$ at pH 4.4 shown in Fig. 4. It shows that the peak centered at 1123 $cm^{-1}$ (stretching Ti–O) disappears and new peaks are located in the 1412–1639 $cm^{-1}$ region. These peaks are attributed to amide C═O, A and C ring C═O, and amide $NH_2$ vibrations of TC [44]. The new absorption peaks are also detected in the TC–$TiO_2$–$SiO_2$ system at pH 4.4 (data not shown) with a smoothly decrease in intensity of the shoulder located at around 960 nm attribute to Ti–O–Si vibrations. The obtained results seem to suggest that the binding of TC to titania (and $TiO_2$–$SiO_2$) is mainly due to electrostatic interactions (and H-bonds formation) between amide, carbonylic and phenolic groups of the antibiotic and the functional groups of $TiO_2$ although weak interactions between TC and $SiO_2$ should not be discarded. These interactions are weaker or less favorable as pH increases.

Table 2 shows the adsorption equilibrium parameters by using the Langmuir and Freundlich isotherms and Table 3 shows the adsorption kinetics parameters by using the pseudo-first-order, pseudo-second-order and pore diffusion models for all experiments. On the one hand, the adsorption isotherms of TC on $SiO_2$ and anatase materials at pH 4.4 were better fitted using the Langmuir than Freundlich adsorption isotherm. This result is expected mainly because the Langmuir's theory assumes monolayer coverage of adsorbate over a homogenous adsorbent surface. On the contrary, the adsorption data points in the TC–$TiO_2$–$SiO_2$ system were fitted using the Freundlich equation which is related to adsorbents with a heterogeneous energy distribution of active sites. The Freundlich parameters also show that the adsorption conditions in all cases are favorable ($n > 1$). On the other hand, the $r^2$ values for the first-order kinetic model are between 0.854 and 0.993 and >0.994 for the pseudo-second-order kinetic model. It is probable, therefore, that this adsorption system is not a pseudo-first-order reaction, it fits the pseudo-second-order kinetic model. In fact, the calculated adsorption amount at equilibrium, $q_e$, obtained in the pseudo-first-order model is inconsistent with the experimental data whereas $q_e$ obtained from pseudo-second-order agrees reasonably well. Thus, the pseudo-second-order model is more suitable to describe the

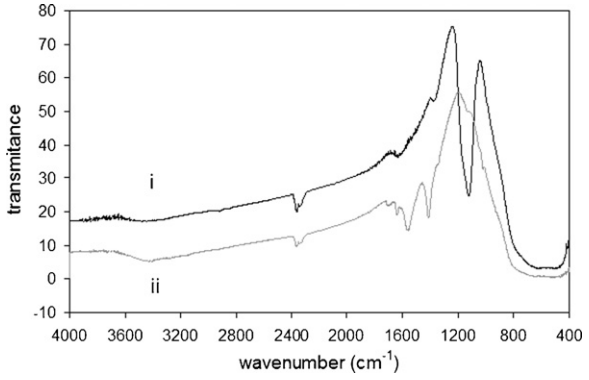


**Fig. 4.** Infrared spectra of (i) $TiO_2$, and (ii) the complex TC–$TiO_2$.

**Table 2**
Parameters of the Freundlich and Langmuir isotherm applied to experimental data for the adsorption of TC on the studied materials.

| | | | | | Freundlich | | | | Langmuir | | | |
|---|---|---|---|---|---|---|---|---|---|---|---|---|
| Sample | %wt $TiO_2$ | pH | T (°C) | IS (M) | $K_F$ | 1/n | n | $r^2$ | $1/q_{mon}$ | $q_{mon}$ (μmolg$^{-1}$) | $K_L$ (μM$^{-1}$) | $r^2$ |
| $SiO_2$ | 0 | 4.4 | 25 | 0 | 0.075 | 0.700 | 1.429 | 0.922 | 0.082 | 12.21 | 0.0025 | 0.996 |
| $TiO_2$-$SiO_2$ | 28 | 4.4 | 25 | 0 | 2.666 | 0.439 | 2.277 | 0.997 | | | | |
| $TiO_2$-$SiO_2$ | 28 | 7.0 | 25 | 0 | 0.688 | 0.533 | 2.134 | 0.968 | | | | |
| $TiO_2$-$SiO_2$ | 28 | 9.5 | 25 | 0 | 0.298 | 0.470 | 2.128 | 0.988 | | | | |
| $TiO_2$-$SiO_2$ | 28 | 4.4 | 15 | 0 | 1.510 | 0.550 | 1.820 | 0.999 | | | | |
| $TiO_2$-$SiO_2$ | 28 | 4.4 | 35 | 0 | 2.238 | 0.479 | 2.089 | 0.994 | | | | |
| $TiO_2$-$SiO_2$ | 28 | 4.4 | 45 | 0 | 2.763 | 0.447 | 2.240 | 0.999 | | | | |
| $TiO_2$-$SiO_2$ | 28 | 4.4 | 25 | 0.01 | 2.426 | 0.424 | 2.361 | 0.999 | | | | |
| $TiO_2$-$SiO_2$ | 28 | 4.4 | 25 | 0.1 | 2.544 | 0.394 | 2.539 | 0.998 | | | | |
| $TiO_2$-$SiO_2$ | 28 | 4.4 | 25 | 0.3 | 2.533 | 0.389 | 2.572 | 0.982 | | | | |
| $TiO_2$-$SiO_2$ | 9 | 4.4 | 25 | 0 | 0.687 | 0.504 | 1.983 | 0.984 | | | | |
| $TiO_2$-$SiO_2$ | 51 | 4.4 | 25 | 0 | 1.526 | 0.470 | 2.128 | 0.993 | | | | |
| $TiO_2$ | | 4.4 | 25 | 0 | 0.773 | 0.530 | 1.885 | 0.992 | | | | |
| $TiO_2$ | | 7.0 | 25 | 0 | 0.321 | 0.523 | 1.912 | 0.965 | | | | |
| $TiO_2$ | | 9.5 | 25 | 0 | 0.312 | 0.556 | 1.798 | 0.982 | | | | |
| $TiO_2$ | | 4.4 | 15 | 0 | 0.567 | 0.653 | 1.531 | 0.998 | | | | |
| $TiO_2$ | | 4.4 | 35 | 0 | 0.852 | 0.491 | 2.035 | 0.994 | | | | |
| $TiO_2$ | | 4.4 | 45 | 0 | 0.785 | 0.475 | 2.107 | 0.970 | | | | |
| $TiO_2$ | | 4.4 | 25 | 0.01 | 0.683 | 0.560 | 1.785 | 0.998 | | | | |
| $TiO_2$ | | 4.4 | 25 | 0.1 | 0.628 | 0.556 | 1.799 | 0.992 | | | | |
| $TiO_2$ | | 4.4 | 25 | 0.3 | 0.751 | 0.537 | 1.861 | 0.999 | | | | |
| anatase | | 4.4 | 25 | 0 | 0.327 | 0.530 | 1.889 | 0.982 | 0.107 | 9.32 | 0.0082 | 0.994 |

adsorption kinetics data. Table 2 also shows the best fitting parameters obtained with the pore diffusion model (Eq. (5)). Even though the formulated model is rather simple, it can fit reasonably well the adsorption behavior of TC on the studied materials.

The effects of temperature on the adsorption of TC on 28 wt% $TiO_2$–$SiO_2$ and $TiO_2$ at pH 4.4 are shown in Fig. 5. TC adsorption on $TiO_2$–$SiO_2$ (Fig. 5a) is not significantly affected by varying the temperature from 15 to 45 °C, and the maximum uptake was between 30 and 32 μmol g$^{-1}$. On the contrary, TC adsorbs negatively on titania as temperature increases (Fig. 5b). Several reports exist about the effect of temperature in the adsorption behavior of TC on different adsorbents. Tanis et al. [45] showed that the adsorption of TC on iron oxides-coated quartz increased by increasing temperature suggesting that a chemisorption-like process may play an important role in the TC-adsorbent system. These observations are significantly different from those reported by Turku et al. [46], who reported that TC adsorption on silica decreased by increasing temperature (physical adsorption). Li et al. [29] showed similar results to those reported by Turku et al. [46] in the TC-kaolinite system at pH higher than p$K_{a2}$ (p$K_{a2}$ = 7.7) whereas the adsorption is not significantly affected by varying the temperature at pH 6 or lower. Therefore, the obtained results suggest that temperature effects on TC adsorption are strongly dependent on the type of adsorbent.

From the data showed in Fig. 5 were obtained the thermodynamic parameters of the Gibbs free energy ($\Delta G^\circ$), enthalpy ($\Delta H^\circ$), and the entropy ($\Delta S^\circ$) of the adsorption of TC onto both adsorbents using the following equations:

$$\Delta G^\circ = -RT \ln\left(\frac{TC_s}{TC_{eq}}\right), \quad (8)$$

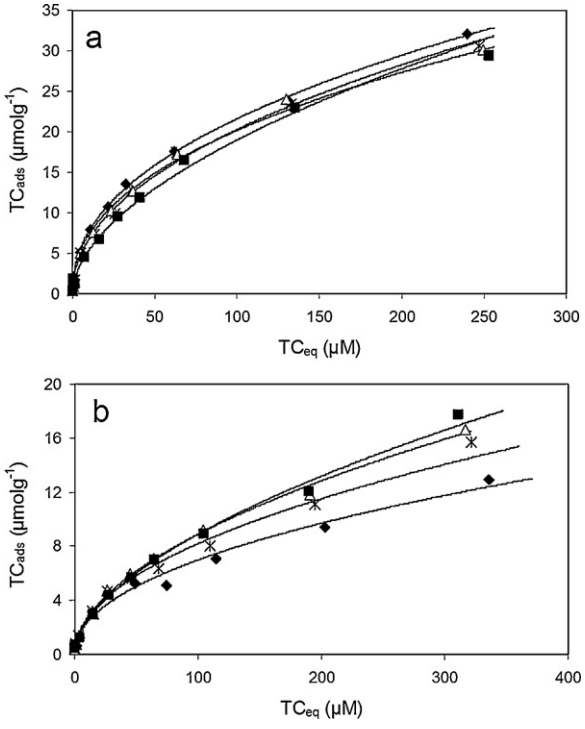


**Fig. 5.** Effect of temperature on the adsorption of TC on (a) 28 wt% $TiO_2$–$SiO_2$, and (b) $TiO_2$ at pH 4.4. Solid squares, 15 °C; open triangles, 25 °C; stars, 35 °C; solid diamonds, 45 °C. Lines show predictions of Eq. (2) with parameters from Table 1.

**Table 3**
Kinetic adsorption parameters obtained using Eqs. (3)–(5).

| | | | | | | pseudo-first-order | | | pseudo-second-order | | | pore diffusion | | |
|---|---|---|---|---|---|---|---|---|---|---|---|---|---|---|
| Sample | %wt $TiO_2$ | $TC_0$ (μM) | pH | T (°C) | IS (M) | $q_e$ (μmolg$^{-1}$) | $k_1$×10$^2$ (min$^{-1}$) | $r^2$ | $q_e$ (μmolg$^{-1}$) | $k_2$×10$^2$ (gμmol$^{-1}$ min$^{-1}$) | $r^2$ | $K_{diff}$ ×10$^2$ (μmolg$^{-1}$min$^{-1/2}$) | I (μmolg$^{-1}$) | $r^2$ |
| $SiO_2$ | 0 | 75 | 4.4 | 25.0 | 0 | 0.31 | 1.08 | 0.933 | 1.96 | 11.55 | 0.999 | 2.36 | 1.57 | 0.947 |
| $TiO_2$-$SiO_2$ | 28 | 2 | 4.4 | 25.0 | 0 | 0.33 | 0.67 | 0.950 | 0.47 | 3.81 | 0.99 | 1.57 | 0.13 | 0.969 |
| $TiO_2$-$SiO_2$ | 28 | 5 | 4.4 | 25.0 | 0 | 0.22 | 0.81 | 0.867 | 0.99 | 9.78 | 1 | 3.48 | 0.55 | 0.995 |
| $TiO_2$-$SiO_2$ | 28 | 10 | 4.4 | 25.0 | 0 | 0.80 | 1.15 | 0.979 | 1.99 | 3.19 | 1 | 11.59 | 0.59 | 0.977 |
| $TiO_2$-$SiO_2$ | 28 | 30 | 4.4 | 25.0 | 0 | 2.39 | 0.83 | 0.990 | 5.32 | 0.67 | 0.999 | 25.26 | 1.57 | 0.978 |
| $TiO_2$-$SiO_2$ | 28 | 50 | 4.4 | 25.0 | 0 | 4.07 | 0.65 | 0.996 | 8.83 | 0.31 | 0.997 | 25.43 | 3.25 | 0.973 |
| $TiO_2$-$SiO_2$ | 28 | 75 | 4.4 | 25.0 | 0 | 5.07 | 0.65 | 0.992 | 11.21 | 0.36 | 0.995 | 27.70 | 5.46 | 0.980 |
| $TiO_2$-$SiO_2$ | 28 | 100 | 4.4 | 25.0 | 0 | 4.16 | 0.73 | 0.995 | 12.97 | 0.52 | 0.998 | 28.13 | 7.08 | 0.974 |
| $TiO_2$-$SiO_2$ | 28 | 75 | 4.4 | 15.0 | 0 | 3.25 | 0.79 | 0.982 | 9.64 | 0.67 | 0.999 | 25.01 | 5.56 | 0.994 |
| $TiO_2$-$SiO_2$ | 28 | 75 | 4.4 | 35.0 | 0 | 4.01 | 0.86 | 0.954 | 10.08 | 0.59 | 0.998 | 18.84 | 6.25 | 0.993 |
| $TiO_2$-$SiO_2$ | 28 | 75 | 4.4 | 45.0 | 0 | 4.80 | 0.87 | 0.982 | 11.04 | 0.46 | 0.997 | 25.88 | 5.97 | 0.996 |
| $TiO_2$-$SiO_2$ | 28 | 75 | 7.0 | 25.0 | 0 | 1.97 | 0.88 | 0.951 | 4.47 | 1.26 | 0.997 | 9.13 | 2.59 | 0.987 |
| $TiO_2$-$SiO_2$ | 28 | 75 | 9.5 | 25.0 | 0 | 1.57 | 0.65 | 0.983 | 3.79 | 1.18 | 0.995 | 8.25 | 2.06 | 0.995 |
| $TiO_2$-$SiO_2$ | 28 | 75 | 4.4 | 25.0 | 0.01 | 4.36 | 0.82 | 0.989 | 9.11 | 0.52 | 0.997 | 21.83 | 4.66 | 0.984 |
| $TiO_2$-$SiO_2$ | 28 | 75 | 4.4 | 25.0 | 0.1 | 4.58 | 0.88 | 0.989 | 9.03 | 0.49 | 0.997 | 21.57 | 4.58 | 0.983 |
| $TiO_2$-$SiO_2$ | 28 | 75 | 4.4 | 25.0 | 0.3 | 4.63 | 0.74 | 0.977 | 9.08 | 0.44 | 0.994 | 21.76 | 4.51 | 0.995 |
| $TiO_2$-$SiO_2$ | 9 | 75 | 4.4 | 25.0 | 0 | 1.44 | 0.91 | 0.912 | 3.36 | 1.79 | 0.996 | 6.30 | 2.05 | 0.987 |
| $TiO_2$-$SiO_2$ | 51 | 75 | 4.4 | 25.0 | 0 | 2.84 | 0.92 | 0.940 | 7.46 | 0.98 | 0.998 | 12.14 | 4.97 | 0.987 |
| $TiO_2$ | | 2 | 4.4 | 25.0 | 0 | 0.35 | 1.89 | 0.903 | 0.37 | 10.85 | 0.997 | 1.09 | 0.16 | 0.972 |
| $TiO_2$ | | 5 | 4.4 | 25.0 | 0 | 0.42 | 1.06 | 0.925 | 0.78 | 4.73 | 0.997 | 3.85 | 0.20 | 0.993 |
| $TiO_2$ | | 10 | 4.4 | 25.0 | 0 | 0.88 | 0.96 | 0.986 | 1.38 | 2.17 | 0.996 | 6.08 | 0.36 | 0.998 |
| $TiO_2$ | | 30 | 4.4 | 25.0 | 0 | 1.78 | 0.87 | 0.964 | 3.15 | 1.12 | 0.997 | 7.30 | 1.55 | 0.993 |
| $TiO_2$ | | 50 | 4.4 | 25.0 | 0 | 1.99 | 0.65 | 0.988 | 4.85 | 0.91 | 0.997 | 9.13 | 2.83 | 0.993 |
| $TiO_2$ | | 75 | 4.4 | 25.0 | 0 | 1.63 | 0.71 | 0.960 | 5.94 | 1.47 | 0.999 | 9.45 | 4.19 | 0.974 |
| $TiO_2$ | | 100 | 4.4 | 25.0 | 0 | 1.26 | 0.78 | 0.974 | 7.18 | 1.96 | 1 | 9.75 | 5.64 | 0.971 |
| $TiO_2$ | | 75 | 4.4 | 15.0 | 0 | 1.47 | 0.84 | 0.980 | 4.33 | 1.89 | 0.998 | 8.13 | 2.75 | 0.973 |
| $TiO_2$ | | 75 | 4.4 | 35.0 | 0 | 2.00 | 0.85 | 0.982 | 4.13 | 1.29 | 0.997 | 11.97 | 2.07 | 0.970 |
| $TiO_2$ | | 75 | 4.4 | 45.0 | 0 | 2.66 | 1.48 | 0.941 | 3.92 | 1.16 | 0.996 | 12.80 | 1.59 | 0.980 |
| $TiO_2$ | | 75 | 7.0 | 25.0 | 0 | 0.37 | 0.75 | 0.990 | 2.80 | 7.64 | 1 | 2.45 | 2.35 | 0.970 |
| $TiO_2$ | | 75 | 9.5 | 25.0 | 0 | 1.49 | 0.65 | 0.984 | 3.55 | 1.48 | 0.996 | 8.23 | 1.89 | 0.985 |
| $TiO_2$ | | 75 | 4.4 | 25.0 | 0.01 | 1.59 | 0.69 | 0.970 | 4.35 | 1.47 | 0.997 | 9.23 | 2.53 | 0.954 |
| $TiO_2$ | | 75 | 4.4 | 25.0 | 0.1 | 1.89 | 1.13 | 0.993 | 4.03 | 1.51 | 0.994 | 8.99 | 2.25 | 0.96 |
| $TiO_2$ | | 75 | 4.4 | 25.0 | 0.3 | 1.89 | 0.86 | 0.941 | 4.54 | 1.35 | 0.996 | 8.85 | 2.75 | 0.97 |
| anatase | | 75 | 4.4 | 25.0 | 0 | 0.35 | 0.91 | 0.976 | 3.04 | 9.19 | 1 | 2.03 | 2.67 | 0.997 |

$$\ln\left(\frac{TC_s}{TC_{eq}}\right) = \frac{\Delta S^\circ}{R} - \frac{\Delta H^\circ}{RT}, \quad (9)$$

where $TC_s$ is the concentration of antibiotic adsorbed (μM), $T$ is the solution temperature in K, and $R$ is the gas constant (8.314 J K$^{-1}$ mol$^{-1}$). The enthalpies of the TC on both solids are obtained from van't Hoff plots as $\ln(TC_s/TC_{eq})$ versus $1/T$. The thermodynamic parameters are shown in Table 4. On the one hand, the $\Delta H^\circ$ value for the adsorption of TC on $TiO_2$ is negative implying that the interaction of TC with the solid is an exothermic process. The low $\Delta H^\circ$ value has been attributed to a number of physical interactions involving electrostatic interactions, ion exchange, water bridging, and hydrogen-type bonding between the TC molecules and the adsorbent structure [47,48]. The negative sorption entropy indicates a decreased randomness at the solid–water interface during TC adsorption. On the other hand, it shows that the value of $\Delta H^\circ$ is positive for 28 wt% $TiO_2$–$SiO_2$. The van't Hoff plots of the interactions of the drug with the surface of the adsorbents require energy and this interaction is endothermic in nature. The positive value of $\Delta S^\circ$ (7.18 J K$^{-1}$ mol$^{-1}$) reflects the affinity of the antibiotic towards solids and may suggest some structural changes in adsorbate (hydration of TC ions) and adsorbent (charged surface upon adsorption) [45]. Finally, the positive value of $\Delta G^\circ$ at various temperatures shows that the nature of adsorption on both adsorbents is not spontaneous.

The apparent activation energy ($E_{app}$) of the process was obtained from kinetic experiments at different reaction temperatures and listed in Table 2. The pseudo-second-order rate constants were used for those purposes by using Arrhenius equation:

$$\ln k_{2,s} = \ln A - \frac{E_{app}}{RT}, \quad (10)$$

where $A$ is the Arrhenius pre exponential term. The slope of plot of $\ln k_{2,s}$ versus $1/T$ is used to evaluate $E_{app}$, which was found to be 9.6 and 12.1 kJ mol$^{-1}$ for 28 wt% $TiO_2$–$SiO_2$ and $TiO_2$, respectively. The low values of $E_{app}$ found here reveal that the adsorption of TC on both solids is controlled by diffusion in aqueous solutions [49]. These results are in agreement with the good fits obtained with the pore diffusion model, i.e., the correlation coefficients were 0.95–1.00 in all experiments.

The effects of the ionic strength on the adsorption isotherm of TC on 28 wt% $TiO_2$–$SiO_2$ at pH 4.4 and 25 °C are shown in Fig. 6. The adsorption equilibrium and adsorption kinetic parameters are shown in Tables 2 and 3, respectively. The adsorption depends on the ionic strength, decreasing as the ionic strength increases. These results suggest that formation of ionic pairs or outer-sphere complexes is the prevailing adsorption process: the competition between TC (as $TC^+$, see Fig. 1) and $K^+$ for negatively charged groups leads to an important decrease in TC adsorption by increasing $K^+$ concentration. Similar results were obtained in the TC–$TiO_2$ system (data not shown), although these effects are less strong than on the titania–silica composed material. Results resemble those reported by Li et al. [29] and Chang et al. [50] for the adsorption of TC on kaolinite and palygorskite, where competition between the antibiotic and electrolyte cations were proposed to play a key role.

Fig. 7 shows the effect of the amount of $TiO_2$ loaded on the silica support on the adsorption of TC at pH 4.4 and 25 °C. The adsorption depends on the $TiO_2$ content, increasing from 0 to 28 wt% $TiO_2$-loading. When titania was loaded at 51 wt%, the tetracycline adsorption capacity decreased. This indicates that there is an optimal $TiO_2$ content that is related to the dispersion of titania crystallites inside mesopores of $SiO_2$. Similar results were reported by Vu et al. [51] on the adsorption of TC on Fe-impregnated SBA-15.

**Table 4**
Thermodynamic parameters of TC adsorption on $TiO_2$ and 28 wt% $TiO_2$–$SiO_2$.

| | 28%wt $TiO_2$-$SiO_2$ | | | $TiO_2$ | | |
|---|---|---|---|---|---|---|
| T (°C) | ΔG° (kJmol$^{-1}$) | ΔH° (kJmol$^{-1}$) | ΔS° (JK$^{-1}$mol$^{-1}$) | ΔG° (kJmol$^{-1}$) | ΔH° (kJmol$^{-1}$) | ΔS° (JK$^{-1}$mol$^{-1}$) |
| 15 | 1.35 | | | 3.11 | | |
| 25 | 1.25 | 3.39 | 7.18 | 3.31 | -10.06 | -45.13 |
| 35 | 1.19 | | | 3.65 | | |
| 45 | 1.00 | | | 4.09 | | |

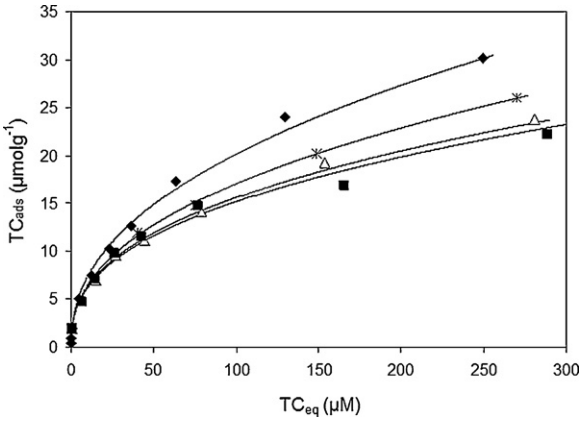


**Fig. 6.** Effect of ionic strength on the adsorption of TC on 28 wt% $TiO_2$–$SiO_2$ at pH 4.4 and 25 °C. KCl concentrations: solid diamonds, 0 M; stars, 0.01 M; open triangles, 0.1 M; solid squares, 0.3 M. Lines show predictions of Eq. (2) with parameters from Table 1.

### 3.3. Photodegradation kinetics

Fig. 8 shows the changes in the UV–VIS spectra of a solution of TC during a typical photodegradation kinetic experiment performed at pH 9.5. This kind of plot was also used to monitor the increase in the concentration of photodegraded TC supernatant ($TC_{photodeg}$) as a function of time in this and all other experiments. In absence of photocatalyst (Fig. 8a), the maximum absorbance of the TC (located at 377 nm) decreases continuously in time and eventually reaches a constant value after 90 min of reaction. The fall in the absorbance at 377 nm is accompanied by an increase in the intensity of the absorption bands located at 237 and 278 nm and the formation of a very strong absorption band at 533 nm. Di Paola et al. [52] revealed that the appearance of this band can be attributed to the formation of 4a, 12a-anhydro-4-oxo-4-dedimethylaminotetracycline. In addition, a well-defined isosbestic point at 427 nm is showed which probably suggests that the herbicide is being degraded into products in a constant relationship. Similar results to those showed at pH 9.5 were reported at pH 7 and 4.4 (data not shown).

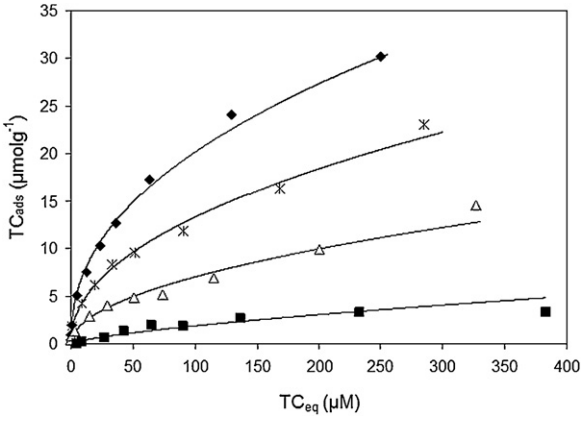


**Fig. 7.** Effect of $TiO_2$-loading on the adsorption of TC on $TiO_2$–$SiO_2$ at pH 4.4 and 25 °C. $TiO_2$-loadings: solid squares, 0 wt%; open triangles, 9 wt%; solid diamonds, 28 wt%; stars, 51 wt%. Lines show predictions of Eq. (2) with parameters from Table 1.

In presence of 50 mg $TiO_2$ (Fig. 8b), a strong decrease in intensity of the maximum absorption band with apparition of the band at 533 nm is observed during the first 55 min of the reaction as similar to those showed in absence of the solid at the same pH. However, after 55 min of UV irradiation, it shows a slightly decrease in the 533 nm band. Similar results were found in $TiO_2$–$SiO_2$ system (data not shown). In presence of anatase (Fig. 8c), the intensity of the 533 nm band strongly decreases with irradiation time up to disappear without the formation of isosbestic points. The obtained result suggests that the products which are stable at pH 9.5 are being degraded to other products in presence of mentioned photocatalysts. It is also possible that this effect would be due to the existence of an alternative degradation mechanism or the existence of several mechanisms in parallel. Fig. 8d shows the change in colour of a TC solution during a typical photodegradation experiment at pH 9.5. At $t = 0$, TC supernatant solution has a fluorescent yellow appearance, at $0 < t < 40$ min the antibiotic solution gradually changes from yellow to fuchsia, and then it discolours. Changes in colour from yellow up to fuchsia were detected in absence and in presence of $TiO_2$ and all titania–silica materials whereas the discolouration was only detected in presence of anatase.

The effect of the studied materials on the photodegradation curves at different pH values and their kinetic parameters are shown in Fig. 9 and Table 5, respectively. To avoid the adsorption effects and quantify only the concentration of photodegraded TC, the experimental results without light were subtracted from those carried out under irradiation. For comparative purposes, solid symbols show the photodegradation curves in absence of photocatalyst. It is noted that the kinetic is strongly dependent of pH, increasing as pH increases. For example, only 90 min were necessary to degrade 85% of initial TC at pH 9.5, whereas at pH 4.4 even after 300 min of reaction only 3% of degradation could be achieved in absence of photocatalyst. However, the catalytic activities of the materials are more effective at lower pH. In fact, the rate increases 12, 18, and 23-fold in presence of 28 wt% $TiO_2$–$SiO_2$ (Fig. 9a), $TiO_2$ (Fig. 9b) and anatase (Fig. 9c) respectively at pH 4.4; it moderately increases (up to 3-fold) at pH 7; and it significantly decreases at pH 9.5 (mainly in $TiO_2$–$SiO_2$ and $TiO_2$) in comparison to those same experiments performed in absence of photocatalyst.

Several reports exist about the effects of titania on the kinetics and mechanism of TC photodegradation [52–56]. It is known that when $TiO_2$ is irradiated with photons of energy equal or

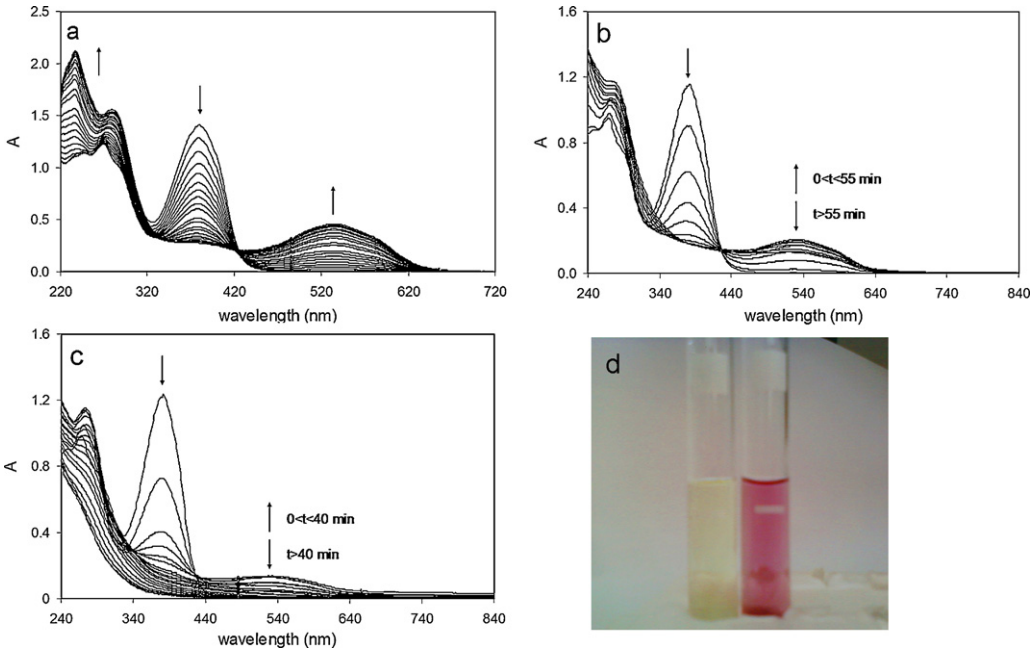


**Fig. 8.** Effect of (a) no catalyst, (b) $TiO_2$, and (c) anatase on the changes of the UV–VIS spectra of the TC supernatant at different reaction times, pH 9.5 and 25 °C. Change in colour of the TC supernatant during a typical photodegradation experiment.

greater than its band-gap energy, the conduction band electrons and valence band holes are generated. The generated holes can either recombine with electrons or react with $OH^-$ or $H_2O$ oxidizing them into $OH^\bullet$ radicals or oxidize the adsorbed TC molecules. The $OH^\bullet$ radicals, together with other highly oxidant species, are responsible for the decomposition of TC [53,55]. Reyes et al. [54] reported that the complete mineralization of TC follows the stoichiometric equation:

$$C_{22}H_{24}N_2O_4 + \frac{45}{2}O_2 \xrightarrow{TiO_2/h\nu} 22CO_2 + 2NH_3 + 9H_2O \quad (11)$$

Addamo et al. [53] showed that during the initial period of the $TiO_2$-assisted photoprocess, the degradation of tetracycline occurs through two competitive reactions: (i) photodeamination and (ii) cleavage of the ring structure. The deamination reaction is probably predominant both in absence or presence of $TiO_2$. The progressive addition of $OH^\bullet$ radicals to the aromatic rings leads to the formation of oxygenated aliphatic intermediates and finally to the formation of $CO_2$. Similar results were reported by Di Paola et al. [52] although they revealed that the treatment with $TiO_2$ (Degussa P-25 and Merck) and UV-light resulting in a complete mineralization

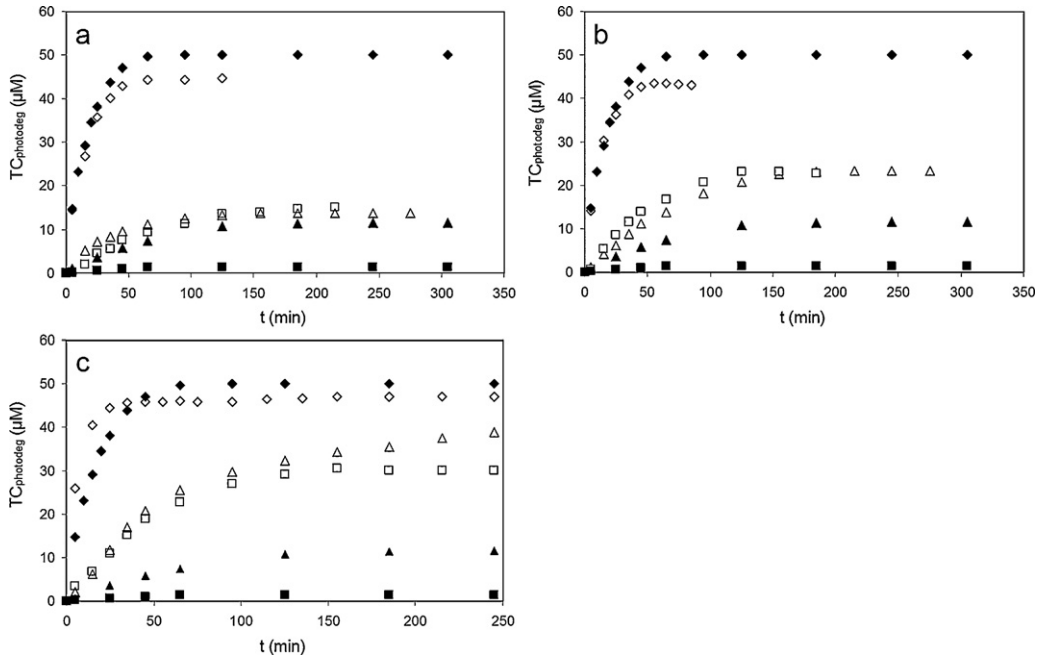


**Fig. 9.** Effect of pH on the photodegradation kinetics of TC. Open symbols show the effects of (a) 28 wt% $TiO_2$–$SiO_2$, (b) $TiO_2$, and (c) anatase on the degradation curves. Solid symbols show the TC degradation in absence of photocatalyst. Studied pH: diamonds, pH 9.5; triangles, pH 7.0; squares, pH 4.4. Initial TC concentration: 60 μM. Mass of photocatalyst: 50 mg.

**Table 5**
Kinetic photodegradation parameters obtained using Eqs. (6) and (7).

| | | | | first-order | | second-order | |
|---|---|---|---|---|---|---|---|
| Sample | %wt $TiO_2$ | Amount (mg) | pH | $k_1 \times 10^3$ ($min^{-1}$) | $r^2$ | $k_2 \times 10^5$ ($\mu M^{-1} min^{-1}$) | $r^2$ |
| | | | 4.4 | 0.28 | 0.988 | | |
| | | | 7.0 | 1.63 | 0.990 | | |
| | | | 9.5 | 35.46 | 0.986 | | |
| $SiO_2$ | | 50 | 4.4 | <0.01 | 0.994 | | |
| $TiO_2$-$SiO_2$ | 28 | 50 | 4.4 | | | 4.42 | 0.997 |
| $TiO_2$-$SiO_2$ | 28 | 50 | 7.0 | | | 9.49 | 0.971 |
| $TiO_2$-$SiO_2$ | 28 | 50 | 9.5 | | | 210.28 | 0.990 |
| $TiO_2$-$SiO_2$ | 28 | 25 | 4.4 | | | 2.77 | 0.989 |
| $TiO_2$-$SiO_2$ | 28 | 100 | 4.4 | | | 5.60 | 0.981 |
| $TiO_2$-$SiO_2$ | 28 | 200 | 4.4 | | | 2.53 | 0.991 |
| $TiO_2$-$SiO_2$ | 9 | 100 | 4.4 | | | 0.87 | 0.989 |
| $TiO_2$-$SiO_2$ | 51 | 100 | 4.4 | | | 5.08 | 1 |
| $TiO_2$ | | 50 | 4.4 | | | 4.71 | 0.997 |
| $TiO_2$ | | 50 | 7.0 | | | 8.63 | 0.996 |
| $TiO_2$ | | 50 | 9.5 | | | 222.38 | 0.990 |
| $TiO_2$ | | 25 | 4.4 | | | 2.56 | 0.980 |
| $TiO_2$ | | 100 | 4.4 | | | 9.52 | 0.970 |
| $TiO_2$ | | 200 | 4.4 | | | 9.10 | 0.980 |
| anatase | | 50 | 4.4 | | | 10.75 | 0.993 |
| anatase | | 50 | 7.0 | | | 22.87 | 0.993 |
| anatase | | 50 | 9.5 | | | 437.93 | 0.984 |
| anatase | | 25 | 4.4 | | | 7.95 | 0.997 |
| anatase | | 100 | 4.4 | | | 16.65 | 0.992 |
| anatase | | 200 | 4.4 | | | 16.16 | 0.989 |

of the antibiotic drug is unlikely. The generation of $OH^{\bullet}$ radicals is favoured as pH increases [57].

From data listed in Table 5, it is observed that the first-order kinetics provide good fit to the experimental data for the TC photodegradation in absence of solids. On the contrary, the second-order kinetic expression with higher $r^2$ values was well fitted in terms of the kinetics of antibiotic degradation by $TiO_2$, $TiO_2$–$SiO_2$, and/or titania. The lower $r^2$ values of the first-order equation were inappropriate to represent the kinetics of photocatalysis of TC by the mentioned materials. The implementation of second-order kinetics to fit experimental data is in agreement to those reported by Kim et al. [58] on the photodegradation of the herbicide metsulfuron methyl onto $TiO_2$ and powdered activated carbon.

Fig. 10 shows the effect of the amount of studied materials on the photodegradation curves at pH 4.4 and 25 °C. The kinetic parameters are shown in Table 5. It clearly shows that the kinetic strongly depends on the amount of added solid, increasing from 0 to 50 mg for the case of 28 wt% $TiO_2$–$SiO_2$ (Fig. 10a). When the amount of titania–silica was higher than 50 mg the photodegradation rate decreased. Similar results were obtained by varying the amounts of $TiO_2$ and anatase (Fig. 10b and c, respectively), i.e., the highest photocatalytic activity occurred at 100 mg in both materials. The obtained results can be explained as follows, the adsorption rate (mainly on $TiO_2$) and photodecomposition rates (upon UV/$TiO_2$) of TC are influenced by the active site and the photo-absorption of the catalyst used. Adequate loading of the semiconductor increases the generation rate of electron/hole pairs for promoting the degradation of the antibiotic drug. However, addition of a high dose of the $TiO_2$ decreases the light penetration due to the higher degree of agglomeration of photocatalyst. These observations are in agreement to those reported by Barakat et al. [59] on the adsorption and photodegradation of Procion yellow H-EXL dye in textile wastewater over $TiO_2$ suspension.

Fig. 11 shows the effect of the $TiO_2$-loading on the photodegradation curves at pH 4.4 and 25 °C. The kinetic parameters are shown in Table 5. The kinetic is strongly dependent on titania content, i.e., the rate strongly increases as the $TiO_2$-loading increases. The increase on the rate is less important at >28 wt% $TiO_2$-loading mainly due to the agglomeration of titania crystallites. At 0 wt%

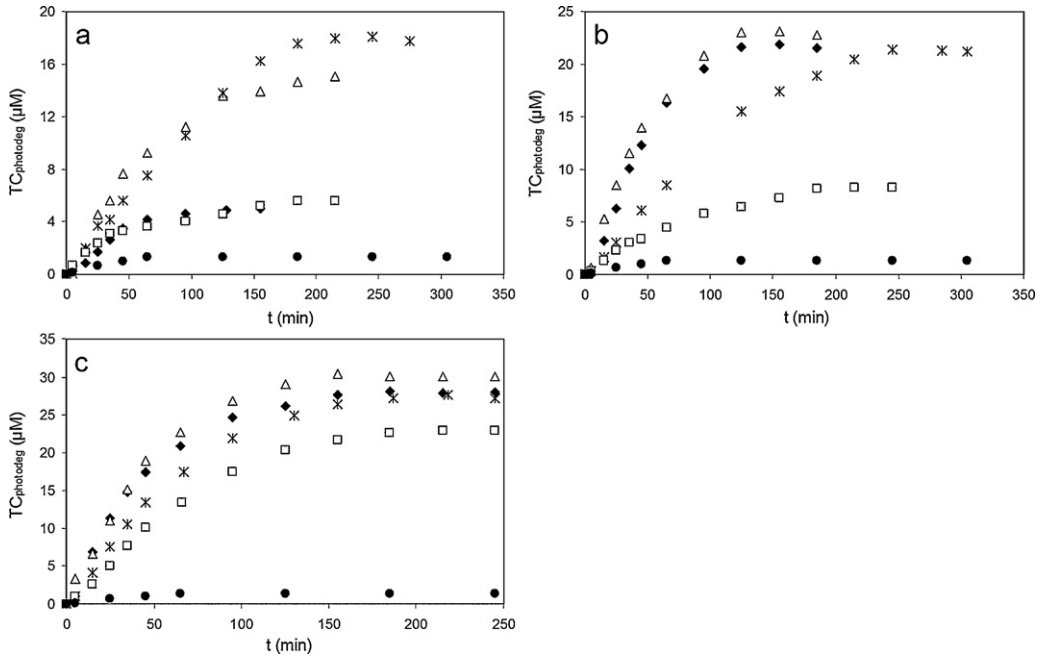


**Fig. 10.** Effect of amount of (a) 28 wt% $TiO_2$–$SiO_2$, (b) $TiO_2$, and (c) anatase on the photodegradation curves at pH 4.4 and 25 °C. Solid circles, no catalyst; open squares, 25 mg; stars, 50 mg; open triangles, 100 mg; solid diamonds, 200 mg. Initial TC concentration: 60 μM.

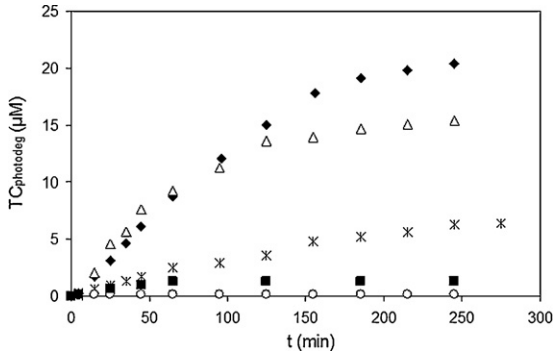


**Fig. 11.** Effect of $TiO_2$-loading on the photodegradation curves at pH 4.4 and 25 °C. $TiO_2$-loadings: solid squares, without solid; open circles, 0 wt%; stars, 9 wt%; open triangles, 28 wt%; solid diamonds, 51 wt%. Initial TC concentration: 60 μM.

$TiO_2$-loading (i.e., $SiO_2$), the rate decreases in comparison to the photodegradation in absence of solid. The obtained results suggest that the silica material protect the antibiotic to be photodegraded, as reported in several works [60,61].

## 4. Conclusions

The results shown in this article reveal that the adsorption of TC on titania and titania–silica is strongly dependent on pH, increasing as pH decreases. The adsorption mechanism, controlled by diffusion processes, is strongly related to electrostatic attractions and H-bond formations mainly between amide, carbonylic and phenolic groups of the antibiotic drug and the functional groups of $TiO_2$. The adsorption capacity at constant pH increases in the order $TiO_2$ < $TiO_2$–$SiO_2$ mainly due to the highly surface area that the silica offers and to the homogenously dispersion of the $TiO_2$ nanocrystallites. The analysis of thermodynamic parameters suggested that the adsorption on $TiO_2$ and 28 wt% $TiO_2$–$SiO_2$ are exothermic and endothermic in nature, respectively.

The obtained results also show that the photodegradation rate is also affected by the presence of $TiO_2$ and $TiO_2$–$SiO_2$ at several pH, although the photocatalytic activities of the studied materials are more important at pH 7 or lower. The photodegradation mechanisms seem to be related to the formation of $OH^{\bullet}$ radicals which are responsible for the decomposition of TC. The photodegradation kinetic at constant pH is strongly dependent on the solid amount and $TiO_2$-loading.

The obtained results have a significant importance in environmental processes, where the production of synthetic materials can play a key role. Mesoporous silica is known to be a very good adsorbent for several species (dyes, pesticides, drugs, heavy metals, etc.) due to the high surface area and pore size. However, since $SiO_2$ could be modified by the incorporation of metal ions or metal oxides on the mesopore structure, the M–$SiO_2$ and/or $MO_x$–$SiO_2$ (M = metal) systems may act not only as excellent adsorbents but also as alternative photocatalysts for pollution control. This will not only benefit the deactivation of the mentioned pollutants but also reduce their leaching and transport through groundwaters.

## Acknowledgments

This work was financed by a grant of the Universidad Nacional del Sur and other of the Agencia Nacional de Promoción de Ciencia y Técnica (ANPCyT). The authors thank Olga Pieroni for the FT-IR spectra. M. Brigante thanks CONICET for the postdoctoral fellowship.

## Appendix A. Supplementary data

Supplementary data associated with this article can be found, in the online version, at doi:10.1016/j.jhazmat.2011.06.082.

## References

[1] Y.J. Wang, D.A. Jia, R.J. Sun, H.W. Zhu, D.M. Zhou, Adsorption and cosorption of tetracycline and copper (II) on montmorillonite as affected by solution pH, Environ. Sci. Technol. 42 (2008) 3254–3259.
[2] B. Halling-Sørensen, S. Nors-Nielsen, P.F. Lanzky, F. Ingerslev, H.C. Holten-Lützhøft, S.E. Jørgensen, Occurrence, fate, and effects of pharmaceutical substances in the environment. A review, Chemosphere 36 (1998) 357–393.

[3] R. Hirsch, T.A. Ternes, K. Haberer, K.L. Kratz, Occurrence of antibiotics in the aquatic environment, Sci. Total Environ. 225 (1999) 109–118.
[4] D.W. Kolpin, E.T. Furlong, M.T. Meyer, E.M. Thurman, S.D. Zaugg, L.B. Barber, H.T. Buxton, Pharmaceuticals, hormones, and other organic wastewater contaminants in U.S. streams, 1999–2000: a national reconnaissance, Environ. Sci. Technol. 36 (2002) 1202–1211.
[5] A.B.A. Boxall, D.W. Kolpin, B. Halling-Sørensen, J. Tolls, Are veterinary medicines causing environmental risks? Environ. Sci. Technol. 37 (2003) 286–294.
[6] H. Schmitt, K. Stoob, G. Hamscher, E. Smit, W. Seinen, Tetracyclines and tetracycline resistance in agricultural soils: microcosm and field studies, Microb. Ecol. 51 (2006) 267–276.
[7] T.A. Ternes, A. Joss, H. Siegrist, Scrutinizing pharmaceuticals and personal care products in wastewater treatment, Environ. Sci. Technol. 38 (2004) 392–399.
[8] L. Ji, F. Liu, Z. Xu, S. Zheng, D. Zhu, Adsorption of pharmaceutical antibiotics on template-synthesized ordered micro- and mesoporous carbons, Environ. Sci. Technol. 44 (2010) 3116–3122.
[9] Z.Y. Hseu, S.H. Jien, S.F. Cheng, Sorption of paraquat on clay components in a Taiwan's oxisol, J. Environ. Sci. Health B 38 (2003) 441–449.
[10] L. Scrano, S.A. Bufo, C. Emmelin, P. Meallier, Abiotic degradation of the herbicide rimsulfuron on minerals and soil, in: E. Lichtfouse, J. Schwarzbauer, D. Robert (Eds.), Environmental Chemistry: Green Chemistry and Pollutants in Ecosystems, Springer, Berlin, 2005, pp. 505–515, cap. 46.
[11] G. Liu, S. Zheng, D. Yin, Z. Xu, J. Fan, F. Jiang, Adsorption of aqueous alkylphenol ethoxylate surfactants by mesoporous carbon CMK-3, J. Colloid Interface Sci. 302 (2006) 47–53.
[12] N.M. Vieno, H. Harkki, T. Tuhkanen, L. Kronberg, Occurrence of pharmaceuticals in river water and their elimination in a pilot-scale drinking water treatment plant, Environ. Sci. Technol. 41 (2007) 5077–5084.
[13] V. Belessi, D. Lambropoulos, I. Konstantinou, R. Zboril, J. Tucek, D. Jancik, T. Albanis, D. Petridis, Structure and photocatalytic performance of magnetically separable titania photocatalysts for the degradation of propachlor, Appl. Catal. B 87 (2009) 181–189.
[14] Y. Zhu, L. Zhang, W. Yao, L. Cao, The chemical states and properties of doped $TiO_2$ film photocatalyst prepared using the Sol–Gel method with $TiCl_4$ as a precursor, Appl. Surf. Sci. 158 (2000) 32–37.
[15] J. Li, S. Liu, Y. He, J. Wang, Adsorption and degradation of the cationic dyes over Co doped amorphous mesoporous titania–silica catalyst under UV and visible light irradiation, Micropor. Mesopor. Mater. 115 (2008) 416–425.
[16] C.T. Kresge, M.E. Leonowicz, W.J. Roth, J.C. Vartuli, J.S. Breck, Ordered mesoporous molecular sieves synthesized by a liquid-crystal template mechanism, Nature 359 (1992) 710–712.
[17] V. Meynen, P. Cool, E.F. Vansant, Verified syntheses of mesoporous materials, Micropor. Mesopor. Mater. 125 (2009) 170–223.
[18] Z.A. AlOthman, A.W. Apblett, Synthesis and characterization of a hexagonal mesoporous silica with enhanced, thermal and hydrothermal stabilities, Appl. Surf. Sci. 256 (2010) 3573–3580.
[19] C. He, B. Tian, J. Zhang, Synthesis of thermally stable and highly ordered bicontinuous cubic mesoporous titania–silica binary oxides with crystalline framework, Micropor. Mesopor. Mater. 126 (2009) 50–57.
[20] M.V.P. Sharma, G. Sadanandam, A. Ratnamala, V.D. Kumari, M. Subrahmanyam, An efficient and novel porous nanosilica supported $TiO_2$ photocatalyst for pesticide degradation using solar light, J. Hazard. Mater. 171 (2009) 626–633.
[21] M.V.P. Sharma, V.D. Kumari, M. Subrahmanyam, $TiO_2$ supported over porous silica photocatalysts for pesticide degradation using solar light: part 2. Silica prepared using acrylic acid emulsion, J. Hazard. Mater. 175 (2010) 1101–1105.
[22] D.M. Antonelli, J.Y. Ying, Synthesis of hexagonally-packed mesoporous $TiO_2$ by a modified sol–gel method, Angew. Chem. Int. Ed. Engl. 34 (1995) 2014–2017.
[23] E. Beyers, P. Cool, E.F. Vansant, Stabilisation of mesoporous $TiO_2$ by different bases influencing the photocatalytic activity, Micropor. Mesopor. Mater. 99 (2007) 112–117.
[24] K.G. Karthikeyan, M.T. Meyer, Occurrence of antibiotics in wastewater treatment facilities in Wisconsin, USA, Sci. Total Environ. 361 (2006) 196–207.
[25] D.W. Kolpin, E.T. Furlong, M.T. Meyer, E.M. Thurman, S.D. Zaugg, L.B. Barber, H.T. Buxton, Pharmaceuticals, hormones, and other organic wastewater contaminants in US streams, 1999–2000: a national reconnaissance, Environ. Sci. Technol. 36 (2002) 1202–1211.
[26] P. Kulshrestha, R.F. Giese Jr., D.S. Aga, Investigating the molecular interactions of oxytetracycline in clay and organic matter: insights on factors affecting its mobility in soil, Environ. Sci. Technol. 38 (2004) 4097–4105.
[27] P.H. Chang, Z. Li, W.T. Jiang, J.S. Jean, Adsorption and intercalation of tetracycline by swelling clay minerals, Appl. Clay Sci. 46 (2009) 27–36.
[28] P.V. Messina, M.A. Morini, M.B. Sierra, P.C. Schulz, Mesoporous silica–titania composed materials, J. Colloid Interface Sci. 300 (2006) 270–278.
[29] Z. Li, L. Schulz, C. Ackley, N. Fenske, Adsorption of tetracycline on kaolinite with pH-dependent surface charges, J. Colloid Interface Sci. 351 (2010) 254–260.
[30] Y.S. Ho, G. Mc Kay, Sorption of dyes and copper ions onto biosorbents, Process Biochem. 38 (2003) 1047–1061.
[31] C.E. Zubieta, P.V. Messina, C. Luengo, M. Dennehy, O. Pieroni, P.C. Schulz, Reactive dyes remotion by porous $TiO_2$–chitosan materials, J. Hazard. Mater. 152 (2008) 765–777.
[32] C.G. Hatchard, C.A. Parker, A new sensitive chemical actinometer. II. Potassium ferrioxalate as a standard chemical actinometer, Proc. R. Soc. Lond. A 235 (1956) 518–536.
[33] G. Gu, P.P. Ong, C. Chu, Thermal stability of mesoporous silica molecular sieve, J. Phys. Chem. Solids 60 (1999) 943–947.
[34] S.R. Yoganarasimhan, C.N.R. Rao, Mechanism of crystal structure transformations. Part 3. Factors affecting the anatase-rutile transformation, Trans. Faraday Soc. 58 (1962) 1579–1589.
[35] J. Yang, J. Zhang, L. Zhu, S. Chen, Y. Zhang, Y. Tang, Y. Zhua, Y. Li, Synthesis of nano titania particles embedded in mesoporous SBA-15: characterization and photocatalytic activity, J. Hazard. Mater. B137 (2006) 952–958.
[36] Q. Zhang, L. Gao, Preparation of oxide nanocrystals with tunable morphologies by the moderate hydrothermal method: Insights from rutile $TiO_2$, Langmuir 19 (2003) 967–971.
[37] H.P. Klug, L.E. Alexander, X-ray Diffraction Procedures, Wiley, NewYork, 1954.
[38] F. Radjy, E.J. Sellevold, A phenomenological theory for the t-method of pore structure analysis: I. Slit-shaped pores, J. Colloid Interface Sci. 39 (1972) 367–378.
[39] A.M. Busuioc-Tomoiagă, M. Mertens, P. Cool, N. Bilba, E.F. Vansant, A simple way to design highly active titania/mesoporous silica photocatalysts, Stud. Surf. Sci. Catal. 74 (2008) 377–380.
[40] K. Gude, V.M. Gun'ko, J.P. Blitz, Adsorption and photocatalytic decomposition of methylene blue on surface modified silica and silica–titania, Colloids Surf. A 325 (2008) 17–20.
[41] V. Zeleňák, V. Hornebecq, S. Mornet, O. Schäf, P. Llewellyn, Mesoporous silica modified with titania: structure and thermal stability, Chem. Mater. 18 (2006) 3184–3191.
[42] R.J. Davies, Z. Liu, Titania–silica: a model binary oxide catalyst system, Chem. Mater. 9 (1997) 2311–2324.
[43] X. Gao, I.E. Wachs, Titania–silica as catalysts: molecular structural characteristics and physico-chemical properties, Catal. Today 51 (1999) 233–254.
[44] C.F. Leypold, M. Reiher, G. Brehm, M.O. Schmitt, S. Schneider, P. Matousek, M. Towrie, Tetracycline and derivatives-assignment of IR and Raman spectra via DFT calculations, Phys. Chem. Chem. Phys. 5 (2003) 1149–1157.
[45] E. Tanis, K. Hanna, E. Emmanuel, Experimental and modeling studies of sorption of tetracycline onto iron oxides-coated quartz, Colloids Surf. A 327 (2008) 57–63.
[46] I. Turku, T. Sainio, E. Paatero, Thermodynamics of tetracycline adsorption on silica, Environ. Chem. Lett. 5 (2007) 225–228.
[47] Z.B. Molu, K. Yurdakoç, Preparation and characterization of aluminum pillared K10 and KSF for adsorption of trimethoprim, Micropor. Mesopor. Mater. 127 (2010) 50–60.
[48] J. Wang, J. Hu, S. Zhang, Studies on the sorption of tetracycline onto clays and marine sediment from seawater, J. Colloid Interface Sci. 349 (2010) 578–582.
[49] D.L. Sparks, Environmental Soil Chemistry, Elsevier, New York, 2003.
[50] P.H. Chang, Z. Li, T.L. Yu, S. Munkhbayer, T.H. Kuo, Y.C. Hung, J.S. Jean, K.H. Lin, Sorptive removal of tetracycline from water by palygorskite, J. Hazard. Mater. 165 (2009) 148–155.
[51] B.K. Vu, E.W. Shin, O. Snisarenko, W.S. Jeong, H.S. Lee, Removal of the antibiotic tetracycline by Fe-impregnated SBA-15, Korean J. Chem. Eng. 27 (2010) 116–120.
[52] A. Di Paola, M. Addamo, V. Augugliaro, E. García-López, V. Loddo, G. Marcì, L. Palmisano, Photolitic and $TiO_2$-assisted photodegradation of aqueous solution of tetracycline, Fresenius Environ. Bull. 13 (2004) 1275–1280.
[53] M. Addamo, V. Augugliardo, A. Di Paola, E. García-López, V. Loddo, G. Marcì, L. Palmisano, Removal of drugs in aqueous systems by photoassisted degradation, J. Appl. Electrochem. 35 (2005) 765–774.
[54] C. Reyes, J. Fernández, J. Freer, M.A. Mondaca, C. Zaror, S. Malato, H.D. Mansilla, Degradation and inactivation of tetracycline by $TiO_2$ photocatalysis, J. Photochem. Photobiol. A: Chem. 184 (2006) 141–146.
[55] Y. Liu, X. Gan, B. Zhou, B. Xiong, J. Li, C. Dong, J. Bai, W. Cai, Photoelectrocatalytic degradation of tetracycline by highly effective $TiO_2$ nanopore arrays electrode, J. Hazard. Mater. 171 (2009) 678–683.
[56] Y. Chen, C. Hu, J. Qu, M. Yang, Photodegradation of tetracycline and formation of reactive oxygen species, in aqueous tetracycline solution under simulated sunlight irradiation, J. Photochem. Photobiol. A: Chem. 197 (2008) 81–87.
[57] C.A. Coutinho, V.K. Gupta, Photocatalytic degradation of methyl orange using polymer–titania microcomposites, J. Colloid Interface Sci. 333 (2009) 457–464.
[58] S.H. Kim, H.H. Ngo, H.K. Shon, S. Vigneswaran, Adsorption and photocatalysis kinetics of herbicide onto titanium oxide and powdered activated carbon, Sep. Purif. Technol. 58 (2008) 335–342.
[59] M.A. Barakat, Adsorption and photodegradation of Procion yellow H-EXL dye in textile wastewater over $TiO_2$ suspension, J. Hydro-environ. Res. 5 (2011) 137–142.
[60] Y. Kohno, S. Tsubota, Y. Shibata, K. Nozawa, K. Yoda, M. Shibata, R. Matsushima, Enhancement of the photostability of flavylium dye adsorbed on mesoporous silicate, Micropor. Mesopor. Mater. 116 (2008) 70–76.
[61] Y. Kohno, K. Totsuka, S. Ikoma, K. Yoda, M. Shibata, R. Matsushima, Y. Tomita, Y. Maeda, K. Kobayashi, Photostability enhancement of anionic natural dye by intercalation into hydrotalcite, J. Colloid Interface Sci. 337 (2009) 117–121.